Hydrazine and Thermal Reduction of Graphene Oxide: Reaction Mechanisms, Product Structures, and Reaction Design

ARTICLE *in* THE JOURNAL OF PHYSICAL CHEMISTRY C · DECEMBER 2009

Impact Factor: 4.77 · DOI: 10.1021/jp909284g

3 AUTHORS, INCLUDING:

Xingfa Gao
Chinese Academy of Sciences
70 PUBLICATIONS **1,322** CITATIONS
SEE PROFILE

Joonkyung Jang
Pusan National University
90 PUBLICATIONS **1,217** CITATIONS
SEE PROFILE

Hydrazine and Thermal Reduction of Graphene Oxide: Reaction Mechanisms, Product Structures, and Reaction Design

Xingfa Gao,[†] Joonkyung Jang,[‡] and Shigeru Nagase*,[†]

Department of Theoretical and Computational Molecular Science, Institute for Molecular Science, Myodaiji, Okazaki 444-8585, Japan, and Department of Nanomaterials Engineering, Pusan National University, Miryang, 627-706, Republic of Korea

Received: September 27, 2009

The density functional theory method (M05-2X/6-31G(d)) was used to investigate reaction mechanisms for deoxygenation of graphene oxides (GOs) with hydrazine or heat treatment. Three mechanisms were identified as reducing epoxide groups of GO with hydrazine as a reducing agent. No reaction path was found for the hydrazine-mediated reductions of the hydroxyl, carbonyl, and carboxyl groups of GO. We instead discovered the mechanisms for dehydroxylation, decarbonylation, and decarboxylation using heat treatment. The hydrazine de-epoxidation and thermal dehydroxylation of GO have opposite dependencies on the reaction temperature. In both reduction types, the oxygen functionalities attached to the interior of an aromatic domain in GO are removed more easily, both kinetically and thermodynamically, than those attached at the edges of an aromatic domain. The hydrazine-mediated reductions of epoxide groups at the edges are suspended by forming hydrazino alcohols. We provide atomic-level elucidation for the deoxygenation of GO, characterize the product structures, and suggest how to optimize the reaction conditions further.

1. Introduction

When sp^2-carbon atoms are arranged into two-dimensional fused hexagons, they form a single-atom-thick allotrope of carbon: graphene. Graphene has been known as the building block of graphite for more than 60 years,[1] but its experimental isolation was first achieved in 2004.[2] Despite its short history of realization, graphene has attracted much attention because of its intriguing crystalline, mechanical, and electronic properties.[3–5] The measurements of elastic properties and intrinsic breaking strength have established graphene as the strongest material ever measured.[6] Reportedly, it has an ultrahigh surface area to mass ratio,[7] and an intrinsic charge mobility that is higher than any semiconductor reported to date.[8] Its band gap[9,10] and magnetic properties[11,12] can be tailored by changing its edge structure and by chemical modification of its interior or edges. These features have made graphene and graphene derivatives ideal for diverse applications such as energy-storage capacitors,[13] sensors,[14] and transistors.[15–18] Graphene has emerged as a "shining star" in materials science.[3–5]

It remains as a challenge to produce high-quality graphene on a large scale. Several laboratory methods have been proposed, each with its own advantages and shortcomings.[2,18–23] Among them, the chemical reduction of *graphene oxide* (GO) yielding *chemically modified graphene* (CMG) has intriguing features: it is cheap and easily scalable to a high-volume production. Particularly, being a solution-based approach, it is well-suited for chemical modification and subsequent processing.[18,19] Consequently, the reduction of GO is widely used for device applications such as preparation of graphene-based composites, thin films, and paper-like materials.[13,14,18,22,24–36] Optimization of reaction conditions has revealed that hydrazine treatment and thermal annealing of GO provide good efficiency for deoxygenation (Table 1).[17,25,36a,37–40] It has also been reported that reduction of GO with $NaBH_4$ followed by treatment with concentrated sulfuric acid and thermal annealing at 1100 °C yields CMG with high purity.[36b]

Oxygen functionalities of four kinds are known to exist in GO: epoxide (−O−), hydroxyl (−OH), carbonyl (−C═O), and carboxyl (−COOH).[41–43] Epoxide and hydroxyl, located on the basal plane of GO, are the major components; carbonyl and carboxyl, distributed at the edges of GO, are minor.[41–43] Gao et al. recently suggested that the presence of five-membered-ring and six-membered-ring lactols at the edges of GO are most likely responsible for the minor oxygen-containing impurities of GO.[36b] After a separate treatment with hydrazine and heat, the oxygen atoms in GO are greatly reduced (Table 1). The CMG obtained from the chemical reduction differs markedly from a defect-free graphene.[2] The CMG includes, apart from the structural disorder and defects inherited from the pristine GO, a large amount of residual oxygen functionality.[35,44–49] For hydrazine reduction, the CMG also contains a considerable amount of N-containing species (Table 1).[47a,48,49] Experimental characterization of the CMG structure and the reduction mechanisms of GO are severely hampered by the amorphous nature of CMG. Stankovich et al.[47a] proposed that the hydrazine-assisted de-epoxidation of GO follows the mechanism shown in Scheme 1. This mechanism nevertheless requires experimental or computational verification. Recently, Kim et al. have studied the epoxide reduction with hydrazine on graphene.[47b] It is also necessary to clarify the reduction mechanisms for other oxygen functionalities of GO. It remains unclear whether the hydroxyl group is removed in the reduction of GO with hydrazine.[47a] The reaction temperature greatly influences the deoxygenation efficiency of GO,[49] but the underlying mechanism is not known. To improve production of graphene-based functional materials via chemical reduction, it is crucial to understand the structure(s) of CMG sheets and their reaction mechanisms.[19]

* To whom correspondence should be addressed. E-mail: nagase@ims.ac.jp.
[†] Institute for Molecular Science.
[‡] Pusan National University.

10.1021/jp909284g
Published on Web 12/04/2009

TABLE 1: Elemental Compositions of GOs before and after Hydrazine and Thermal Reduction

reduction process	GO (before reduction)	CMG (after reduction)	ref
hydrazine hydride is added to an aqueous GO solution, then the system is kept at 100 °C for 1 day	C:O:N = 2.7:1:0	C:O:N = 10.3:1:0.6	ref 47a
GO film is dispersed and stirred in anhydrous hydrazine (98%) for 1 week; the resulting hydrazinium graphene suspension is spin-coated onto a Si/SiO_2 substrate and thermally annealed at 150 °C	C:O:N = 1.3:1:0	C:O:N = 7.7:1:1.4 (before annealing); C:O:N = 12:1:0.7 (after annealing)	ref 48
GO film on Si_3N_4/Si substrate is annealed at 900 °C in ultrahigh vacuum for 15 min	C:O = 2.8:1	C:O = 14.1:1	ref 49

SCHEME 1: Mechanism Proposed in Reference 47a for the De-epoxidation of GO with Hydrazine

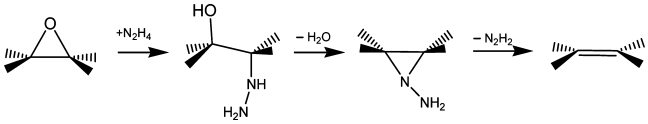

In this article, using the density functional theory method, we investigate the reactions of four oxygen functionalities of GO systematically under hydrazine and heat treatment conditions. More specifically, attempts are made to answer the questions presented in Figure 1.[19] Our results provide atomistic details for deoxygenation of GO via hydrazine and heat treatments. We also suggest methods to optimize the deoxygenation conditions of GO.

2. Computational Details

2.1. GO Models. Experimentally available GOs are amorphous materials with large sizes. Their stoichiometries and structures vary depending on the methods used for their syntheses.[41,47a,50] Microscopic image[44,45,51] and Raman spectroscopy[28] have shown that oxygen functionalities form islands and lines on the basal plane of GO, dividing the GO sheet into small in-plane aromatic domains (Figure 2). Therefore, we model the local surface structures of GO as fragmental graphene sheets modified with oxygen functionalities. A similar model has been used to compute the erosion and combustion of graphite. The model was verified as reliable through comparison with experiments.[51,52] We investigated the surface-size effects on the reduction of GO by systematically increasing the model sheet size.

The epoxide groups of GO are classified into two types: epoxides that are located at the interior of an aromatic domain of GO, and epoxides located at the edges of an aromatic domain. The edges are an important determinant of the reactivity of graphene nanosheets.[53] The same classification is applicable to the hydroxyl groups of GO. Therefore, the oxygen functionalities of GO are of six types, as presented in Figure 2: **A**, **A′**, **B**, **B′**, **C**, and **D**. We use various cluster models of GO for oxygen functionalities of these six types (Chart 1). Models **3a**, **4a**, and **5a** are for GO with the oxygen functionality **A**. **1b**, **2b**, **4b**, and **5b** mimic GOs with oxygen functionality **A′**. **5c**−**f** and **6a** are models for GO with functionality **B**. Both **5g** and **5h** are models of GO with functionality **B′**. Models **6a** and **4c** are respectively the models of GOs with carbonyl and carboxyl groups. The aromatic domains of **3a**, **4a**, and **5a** gradually become larger, as do those of **1b**, **2b**, **4b**, and **5b**. These two sets are used to investigate the size effect on the de-epoxidation of GO. The hydroxyl groups of **5c**−**f** gradually move away from the interior to the edge of **5**. Therefore, **5c**−**f** are used to investigate the edge effect on the dehydroxylation of GO.

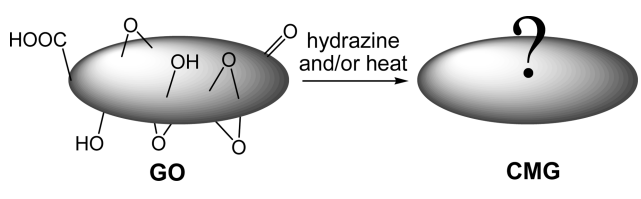

Figure 1. Schematic illustration of questions addressed in this article.

2.2. Computational Methods. All calculations were performed with the GAUSSIAN 03 program.[54] Geometry optimizations for all stationary points (energy minima and transition states) were done with the M05-2X[55] density functional combined with the 6-31G(d)[56,57] basis set. For all optimized geometries, we did frequency analyses at the same level of theory (M05-2X/6-31G(d)) to calculate entropies (*S*), enthalpies (*H*), and Gibbs free energies (*G*). We characterized all transition states as geometries exhibiting only one imaginary frequency, and all energy minima as geometries without imaginary frequencies. For each representative reaction path, we performed an intrinsic reaction coordinate (IRC) calculation at the level of M05-2X/6-31G(d) to verify that the transition states are directed correctly toward the energy minima. We applied a spin-unrestricted M05-2X (UM05-2X) method for radical species of **5c**−**h**, **6**, OH radical, and the transition states for dehydroxylations of **5c**−**h** and **6a**. We used a spin-restricted M05-2X (RM05-2X) method to calculate the other closed-shell singlet species. The transition state for the dehydroxylation of **6a** has an open-shell singlet ground state. Therefore, an initial guess with broken symmetry was used for the calculation of this transition state. To obtain an energy in the presence of solvent, we applied the single-point energy calculation using the PCM

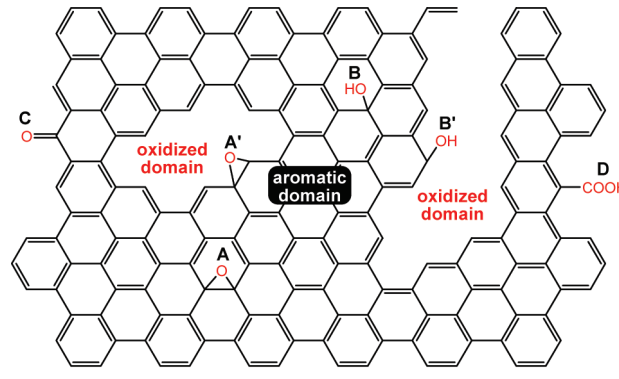

Figure 2. Schematic illustration of oxygen-containing groups in GO: **A**, epoxide located at the interior of an aromatic domain of GO; **A′**, epoxide located at the edge of an aromatic domain; **B**, hydroxyl located at the interior of an aromatic domain; **B′**, hydroxyl at the edge of an aromatic domain; **C**, carboxyl at the edge of an aromatic domain; and **D**, carboxyl at the edge of an aromatic domain.

CHART 1: Fragmental Graphene and GO Sheets[a]

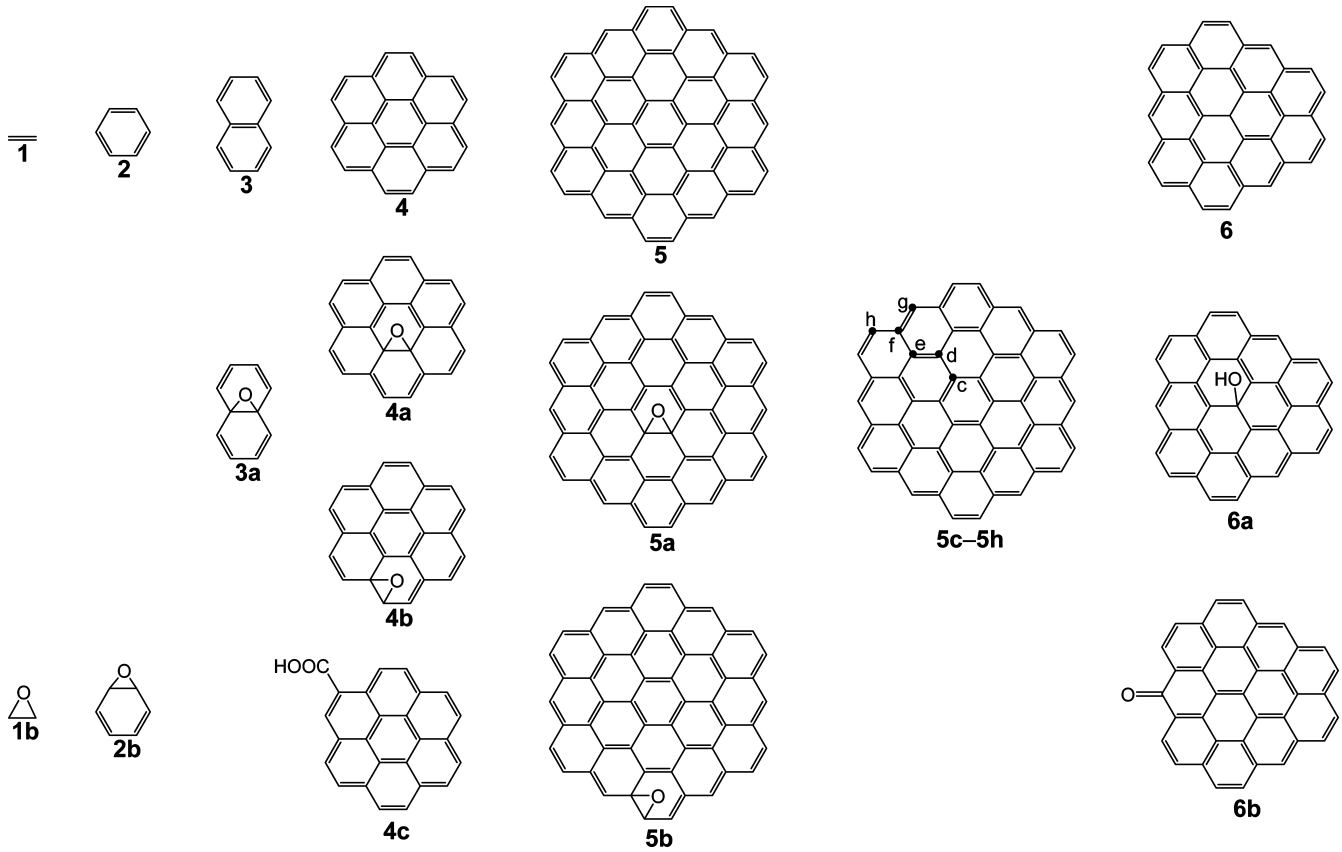

[a] Here, **1**−**6** are fragments of graphene. **3a**, **4a**, and **5a** have epoxides on the basal planes of graphene sheets. **1b**, **2b**, **4b**, and **5b** have epoxides at the edges of aromatic domains. **6a** and **5c**−**h** have hydroxyl groups. Drawn as black circles in **5c**−**h** are the positions to which the hydroxyl groups are attached. Both **4c** and **6b** have carboxyl and carbonyl groups. Hydrogen atoms are omitted in the figure for clarity.

model[58] and the M05-2X/6-31G(d) method for the geometry optimized without solvent.

Reportedly, the M05-2X density functional is accurate in calculating bond dissociation energies.[55] To confirm the accuracy of the M05-2X/6-31G(d) in predicting the reduction kinetics of GO, we calculated the reaction energy profile for the hydrazine reduction of **2b** using two methods: M05-2X/6-31G(d) and CCSD(T)[59]/cc-pVDZ.[60] The results are depicted in Figure 3. Both methods predict similar reaction energy profiles (Figure 3). Consequently, M05-2X/6-31G(d) is a computationally efficient method with moderate accuracy that is practically feasible for studying the deoxygenation mechanisms of GO with treatment of hydrazine and heat.

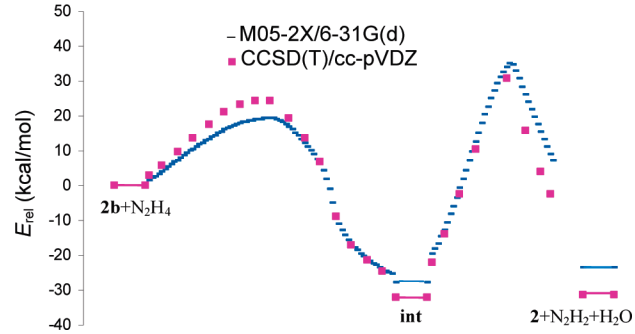

Figure 3. Reaction energy profiles for the hydrazine de-epoxidation of **2b** via Route 2 (Scheme 2), calculated using M05-2X/6-31G(d) and CCSD(T)/cc-pVDZ. In both calculations, geometries of the stationary points were optimized at the level of M05-2X/6-31G(d). Geometries between stationary points were optimized by following the intrinsic reaction coordinates with a step size of 0.015 amu$^{1/2}$·Bohr, using the same level of theory. The energy profile at the level of CCSD(T)/cc-pVDZ was obtained with single-point energy calculations based on the M05-2X/6-31G(d) geometries.

3. Results and Discussion

3.1. Mechanisms of Hydrazine De-epoxidation under Vacuum. We found three reaction routes—Routes 1, 2, and 3—for removal of the epoxide group in GO using hydrazine as a reducing agent under vacuum (Scheme 2). In contrast, we have not found the mechanism of Scheme 1.[47a] In Route 1 of Scheme 2, de-epoxidation occurs in three steps: First, hydrazine (N_2H_4) attacks the carbon of epoxide from the back side of the epoxide ring. This step opens the ring of epoxide and forms **int$_1$**. Second, the C−C bond of **int$_1$** rotates to bring the hydrazine group (−H_2NNH_2) attached to the opposite side of the oxygen close to the oxygen. Then one H-atom transfers from the hydrazine group to the oxygen of epoxide, forming a hydrazino alcohol **int$_2$**. Third, another H of **int$_2$** transfers from the hydrazino group (−$HNNH_2$) to the hydroxyl group (−OH). This gives a water molecule (H_2O), a *cis*-diazene (*cis*-N_2H_2), and the deoxygenated product. In Route 2, the de-epoxidation proceeds in two steps: First, N_2H_4 attacks the sp^2-carbon nearest to the epoxide group from the front side of the epoxide ring. One H is transferred from N_2H_4 to the epoxide, yielding **int**. The second step progresses similarly to the third step of Route 1 to give H_2O and *cis*-N_2H_2 and finish the deoxygenation. In Route 3, de-epoxidation occurs in three steps. First, N_2H_4 attacks the sp^2-carbon located at the meta position of epoxide to give **int$_1$**. Second, the −OH and −$HNNH_2$ groups of **int$_1$** rotate in a

SCHEME 2: GO Reduction Mechanisms[a]

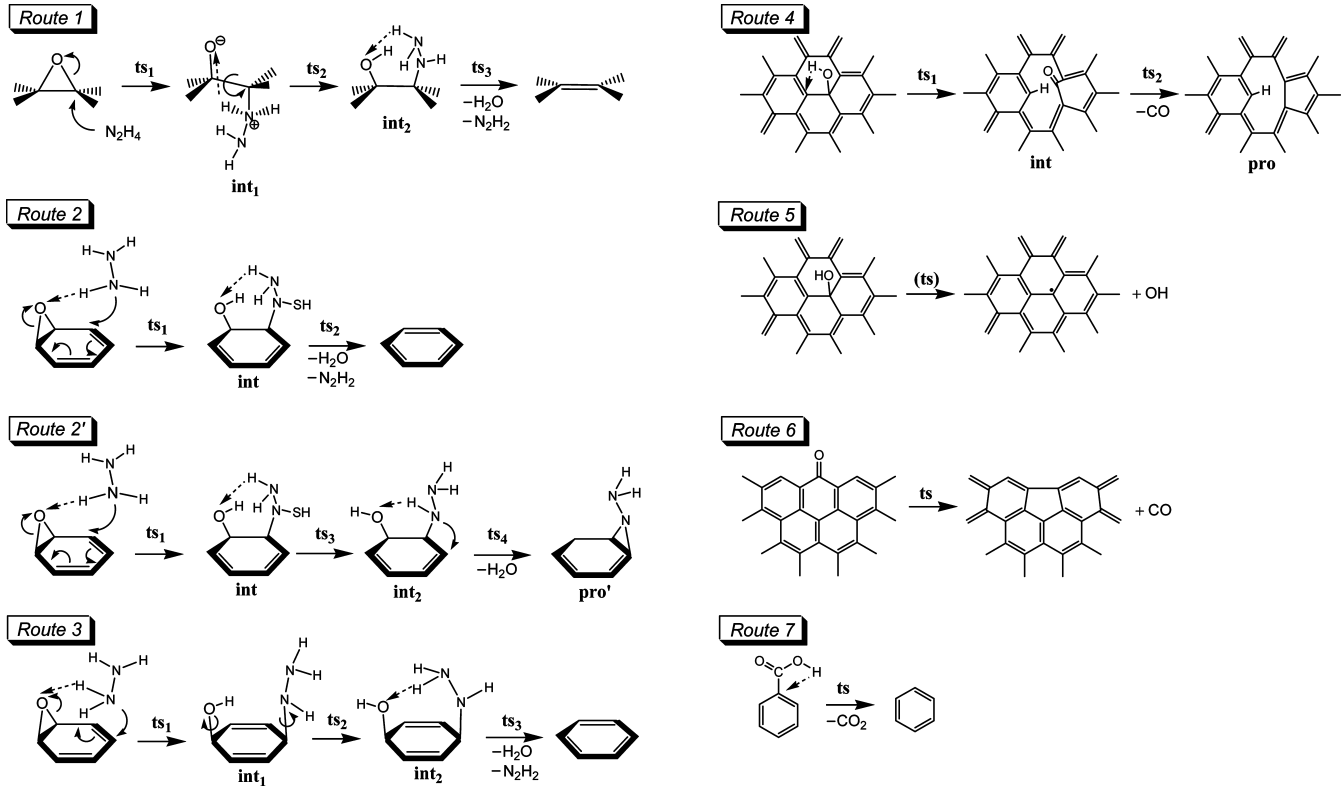

[a] Routes 1−3 and 2′ represent the mechanisms for the hydrazine de-epoxidation of GO. Routes 4 and 5 refer to the mechanism for the thermal de-hydroxylation of GO. Routes 6 and 7 respectively show the mechanisms for thermal de-carbonylation and thermal de-carboxylation of GO.

disrotatory mode, converting **int$_1$** to **int$_2$**. The third step is similar to the third step of Route 1.

The hydrazine de-epoxidation of **1b** follows Route 1, whereas those of **3a**, **4a**, **5a**, **2b**, **4b**, and **5b** follow either Route 2 or Route 3. Figure 4 presents the reaction energy profiles for the reductions of **5a** and **5b**. Figure 5 portrays the three-dimensional atomic structures for the stationary points involved in the hydrazine reduction of **5a**. Table 2 presents the energies of the stationary points in the reductions of **3a**, **4a**, **2b**, **4b**, and **1b**.

Table 2 shows that for the hydrazine de-epoxidation of **3a** via Route 2 under vacuum, the second step (second H-transfer) is the rate-determining step. This step has a Gibbs free-energy barrier of 51.1 kcal/mol at room temperature ($G^{\ddagger}_{25°C}$ = 45.3 − (−5.8) = 51.1 kcal/mol) (Table 2). For the de-epoxidation of **3a** via Route 3 under vacuum, the first step (the first H-transfer) is rate determining, with $G^{\ddagger}_{25°C}$ = 48.3 kcal/mol (Table 2). Therefore, Route 3 is slightly more efficient than Route 2 for the hydrazine reduction of **3a**. In the hydrazine de-epoxidation of **4a** (**5a**), the first step (first H-transfer) is rate determining, irrespective of via Route 2 or Route 3. However, the de-epoxidation of **4a** (**5a**) via Route 2 has $G^{\ddagger}_{25°C}$ of 41.2 (34.9) kcal/mol. This barrier is lower than the corresponding barrier in Route 3, which is 49.3 (38.0) kcal/mol (Table 2 and Figure 4). Therefore, Route 2 is kinetically more favorable than Route 3 in the de-epoxidation of **4a** (**5a**) with hydrazine. These results suggest that Route 3 dominates hydrazine reductions when the epoxides being attacked are located at the interior of a small aromatic domain, but Route 2 is expected to prevail if those interior epoxides belong to a large aromatic domain.

Table 2 and Figure 4 show that hydrazine reductions of **3a**, **4a**, and **5a** are exothermic. The enthalpy changes (ΔH) for **3a**, **4a**, and **5a** are respectively −33.6, −46.1, and −41.5 kcal/mol. The corresponding changes in the Gibbs free energy at room temperature ($\Delta G_{25°C}$)—given respectively as −4.1, −57.0, and −53.2 kcal/mol—are even more negative. Meanwhile, the intermediates involved in these reductions, the hydrazino alcohols, are thermally much less stable than the corresponding reduction products. The hydrazine de-epoxidations of **3a**, **4a**, and **5a** are therefore thermodynamically spontaneous processes. However, the reaction energy barriers ($G^{\ddagger}_{25°C}$) for these processes are respectively 48.3, 41.2, and 34.9 kcal/mol. The energy barriers for **3a**, **4a**, and **5a** suggest that the hydrazine reduction of epoxide becomes more favorable if it belongs to a larger aromatic domain. Consequently, epoxides at the interior of an aromatic domain of GO will be removed by hydrazine at reaction temperatures of 100−150 °C.[47a,48]

Table 2 and Figure 4 show that the first H-transfer is the rate-determining step in the hydrazine de-epoxidations of **4b** and **5b** via Route 3, whereas the second H-transfer is rate determining in the other de-epoxidations. The $G^{\ddagger}_{25°C}$ values for the de-epoxidations of **2b**, **4b**, and **5b** via Route 2 are 60.7, 68.8, and 71.7 kcal/mol, respectively; those via Route 3 are 44.0, 63.2, and 70.2 kcal/mol, respectively. Therefore, the kinetically favorable pathways for hydrazine reductions of **2b**, **4b**, and **5b** should follow respectively Routes 3, 2, and 2. In contrast, the de-epoxidation of **1b** with hydrazine exclusively follows Route 1 with $G^{\ddagger}_{25°C}$ = 83.5 kcal/mol (Table 2).

Hydrazine de-epoxidations of **1b**, **2b**, **4b**, and **5b** exhibit features that differ from those of **3a**, **4a**, and **5a**. In fact, the $\Delta G_{25°C}$ values for these are −2.3 to −34.6 kcal/mol and are less negative than those for **3a**, **4a**, and **5a** (Table 2 and Figure 4). The de-epoxidations of **1b**, **4b**, and **5b** involve stable hydrazino alcohol intermediates: **int$_2$** for **1b**, **int** for **4b**, and **int** for **5b**. These intermediates have Gibbs free energies of formation of −25.2, −21.6, and −29.8 kcal/mol at room temperature, respectively, which are even lower than those for

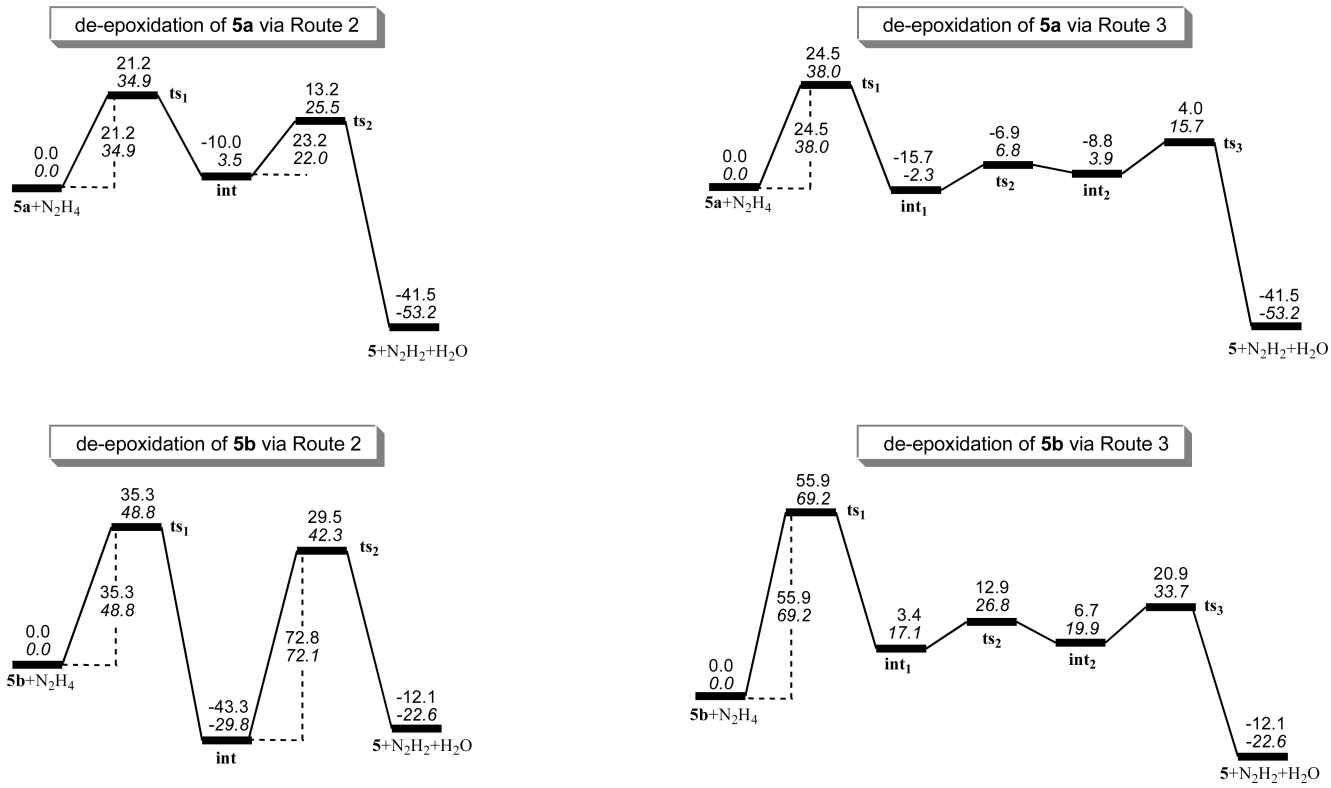

Figure 4. Reaction energy profiles for hydrazine de-epoxidations of **5a** and **5b** under vacuum calculated at the M05-2X/6-31G(d) level of theory. Values in normal and italic typefaces are respectively relative enthalpies (H_{rel}, in kcal/mol) and relative Gibbs free energies (G_{rel}, in kcal/mol) at room temperature (25 °C).

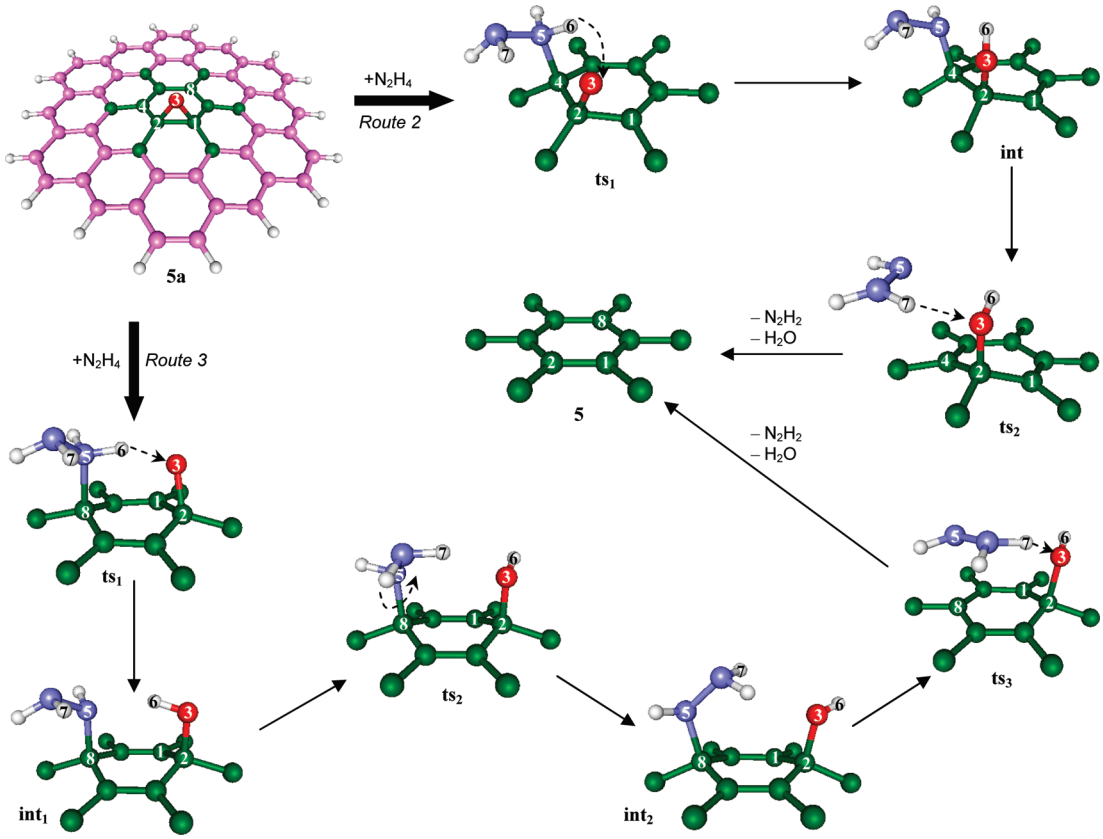

Figure 5. Local atomic structures for stationary points involved in hydrazine de-epoxidations of **5a** via Routes 2 and 3.

the corresponding reduction products (i.e., −0.4, −20.6, and −22.6 kcal/mol) (Table 2 and Figure 4). Therefore, the hydrazine de-epoxidation for **1b**, **4b**, and **5b** will stop with the formation of a hydrazino alcohol. The reaction energy barriers ($G^{\ddagger}_{25°C}$) for the de-epoxidations of **2b**, **4b**, and **5b** are 44.0, 62.5, and 69.2 kcal/mol, respectively, showing an increasing behavior

TABLE 2: Reaction Enthalpies (kcal/mol) and Gibbs Free Energies (25 °C, in Parentheses, kcal/mol) for Stationary Points Involved in Hydrazine De-epoxidations of 3a, 4a, 1b, 2b, and 4b under Vacuum at the M05-2X/6-31G(d) Level of Theory[a]

		de-epoxidation via Route 2			de-epoxidation via Route 3					
	reactant	**ts$_1$**	**int**	**ts$_2$**	**ts$_1$**	**int$_1$**	**ts$_2$**	**int$_2$**	**ts$_3$**	product
3a + N_2H_4	0.0 (0.0)	29.1 (42.4)	−18.1 (−5.8)	33.1 (45.3)	35.8 (48.3)	−15.2 (−2.5)	−8.0 (4.9)	−17.6 (−5.6)	17.1 (29.6)	−33.6 (−44.1)
4a + N_2H_4	0.0 (0.0)	27.1 (41.2)	−8.5 (4.9)	9.6 (22.4)	35.6 (49.3)	2.2 (15.5)	10.7 (24.3)	8.0 (20.8)	11.0 (23.8)	−46.1 (−57.0)
2b + N_2H_4	0.0 (0.0)	20.0 (33.6)	−28.8 (−16.7)	32.2 (44.1)	25.9 (38.5)	−24.3 (−11.9)	−20.2 (−7.7)	−25.8 (−13.9)	17.8 (30.1)	−22.1 (−33.1)
4b + N_2H_4	0.0 (0.0)	35.4 (47.8)	−34.4 (−21.6)	43.9 (58.9)	49.8 (62.5)	0.3 (13.3)	9.5 (22.5)	3.3 (15.9)	21.0 (33.9)	−9.5 (−20.6)

		de-epoxidation via Route 1					
	reactant	**ts$_1$**	**int$_1$**	**ts$_2$**	**int$_2$**	**ts$_3$**	product
1b + N_2H_4	0.0 (0.0)	36.0 (47.6)	33.1 (44.7)	35.0 (47.4)	−37.2 (−25.2)	46.5 (58.4)	9.7 (−0.4)

[a] For definitions of **3a**, **4a**, **1b**, **2b**, and **4b**, see Chart 1; for definitions of Routes 1−3, see Scheme 2.

concomitantly with increased size of aromatic domain. Consequently, hydrazine reductions of epoxides located at the edges of GO become increasingly difficult as the aromatic domain size increases.

3.2. Mechanisms of Thermal Dehydroxylation under Vacuum. We have found no reaction route corresponding to the reduction of the hydroxyl group of GO with hydrazine as a reducing agent. Hydrazine plays a minor role, if any, in the dehydroxylation of GO. Instead, we have located two reduction routes without hydrazine: Routes 4 and 5 (Scheme 2). In Route 4, the hydroxyl reduction takes place in two steps and yields a monoxide (CO) and a graphene sheet with a vacancy. By contrast, in Route 5, the hydroxyl group directly leaves the graphene sheet, producing an OH radical and a graphene radical. Xu et al.[61] studied the dissociative adsorption of an OH radical on graphite surfaces. They reported similar routes for the reaction of an OH radical with their model graphite.[61]

Figure 6a depicts the reaction energy profile for reductions of **6a** via Routes 4 and 5. They are respectively both endothermic with ΔH = 99.0 and 30.1 kcal/mol. The corresponding $\Delta G_{25°C}$ and $G^{\ddagger}_{25°C}$ values are respectively 85.5 and 18.1 kcal/mol, and 89.9 and 27.7 kcal/mol. Given the significantly higher values in $G^{\ddagger}_{25°C}$ and $\Delta G_{25°C}$, Route 4 is expected to be much less competitive than Route 5 in the thermal reduction of hydroxyl groups of GO, which accords with the results of Xu et al.[61] We will therefore not consider Route 4 in the following discussions.

We studied the dehydroxylations of **5c**−**h** via Route 5 to investigate the manner in which dissociation energies depend on the positions of hydroxyl groups of GO. The hydroxyl groups of **5c**−**h** increasingly move their positions away from the interior toward the edges of **5** (Chart 1). The reaction energy profiles are depicted in Figure 6b. The dehydroxylation of **5c** (**5d**−**f**) via Route 5 has a transition state with $G^{\ddagger}_{25°C}$ of approximately 13.8 kcal/mol; the dehydroxylation of **5g** (**5h**) via Route 5 involves no transition state (Figure 6b). Figure 6b presents that all dehydroxylations of **5c**−**h** are endothermic with ΔH values of 7.2−35.6 kcal/mol. In addition, $\Delta G_{25°C}$ values for **5c**−**h** are respectively −3.3, −3.5, −3.1, −2.7, 25.8, and 16.5 kcal/mol. A negative $\Delta G_{25°C}$ and a low $G^{\ddagger}_{25°C}$ for **5c**−**e** suggest that a single hydroxyl group attached to the interior aromatic domain of **5** (i.e., **5c**−**f**) is not stable and is subject to dissociation at room temperature. In contrast, a positive $\Delta G_{25°C}$ for **5g** and **5h** suggests that a hydroxyl attached at the edge of **5** is stable at room temperature. Hydroxyls attached to the inner aromatic domains of GO are therefore expected to dissociate or migrate to the edges of aromatic domains. We further investigate how to reduce hydroxyls at the edges of aromatic domains of GO (see below).

3.3. Mechanisms of Thermal Decarbonylation and Decarboxylation under Vacuum. We have not found reaction routes for which the carbonyl and carboxyl groups of GO are removed with hydrazine treatment. As in dehydroxylation, hydrazine will not play an important role in the decarbonylation

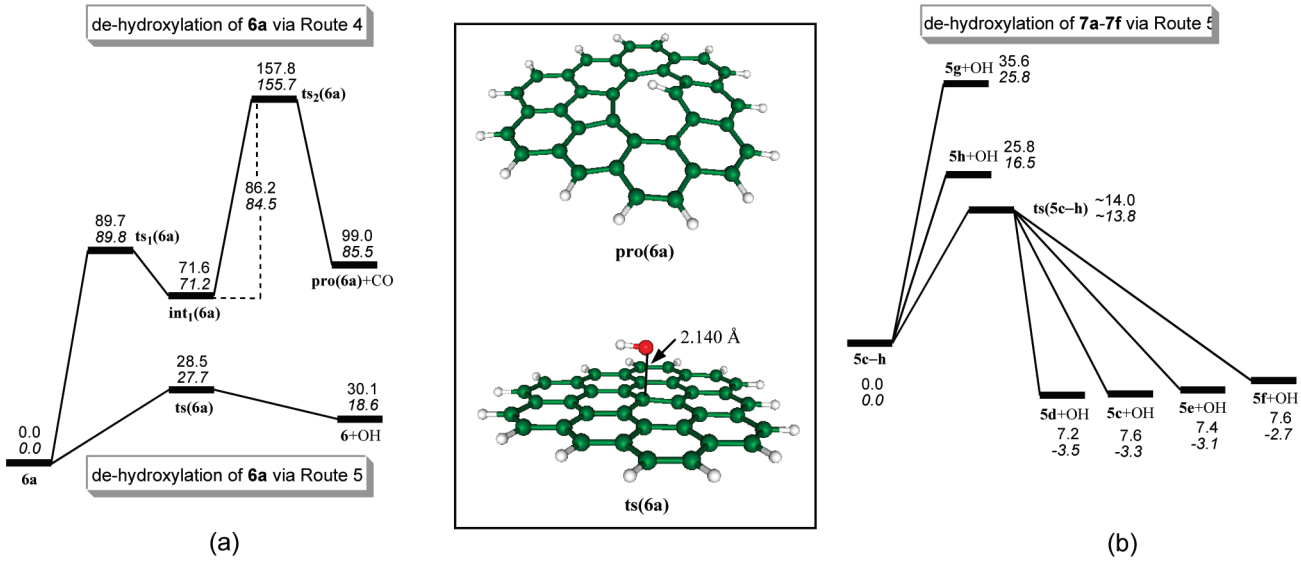

Figure 6. Reaction energy profiles for the dehydroxylation of (a) **6a** and (b) **5c**−**h** under vacuum obtained from the M05-2X/6-31G(d) level of theory. Values in normal and italic print respectively show relative enthalpies (H_{rel}, in kcal/mol) and relative Gibbs free energies (G_{rel}, in kcal/mol) at room temperature (25 °C). The inset presents schematic structures of **pro**(**6a**) and **ts**(**6a**).

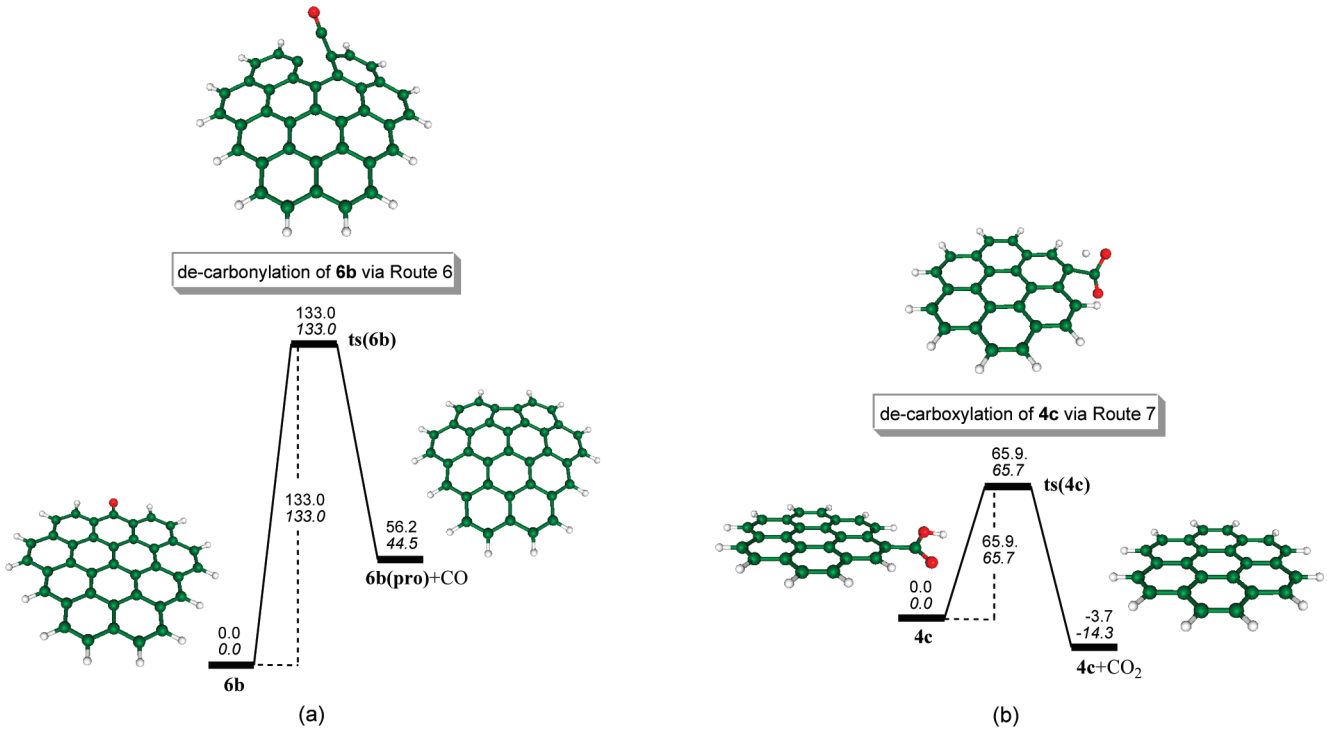

Figure 7. Reaction energy profiles for (a) decarbonylation of **6b** and (b) decarboxylation of **4c** under vacuum. Calculation used the M05-2X/6-31G(d) level of theory. Values in normal and italic print typefaces respectively depict relative enthalpies (H_{rel}, in kcal/mol) and relative Gibbs free energies (G_{rel}, in kcal/mol) at room temperature (25 °C). Schematic structures of stationary points are also shown.

or decarboxylation of GO. However, we found reaction routes without hydrazine, which correspond to thermal decarbonylation and decarboxylation of GO under vacuum: Routes 6 and 7 (Scheme 2). Both routes involve one-step deoxygenation with a transition state.

Figure 7a presents the reaction energy profile for the decarbonylation of **6b** via Route 6. The thermal decarbonylation under vacuum is endothermic (ΔH = 56.2 kcal/mol). The corresponding $\Delta G_{25°C}$ and $G^{\ddagger}_{25°C}$ values are 44.5 and 133.0 kcal/mol, respectively, meaning that the decarbonylation of **6b** via Route 6 does not occur spontaneously at room temperature. Furthermore, hydrazine can add to the C═O double bond of **6b**, forming a hydrazino alcohol (Figure S1 of the Supporting Information). This addition reaction has a positive $\Delta G_{25°C}$ as well ($\Delta G_{25°C}$ = 6.7 kcal/mol) and is not spontaneous. This addition reaction involves a decrease in entropy ($\Delta S < 0$). Therefore, the increased reaction temperature will make ΔG more positive. This addition reaction will not occur spontaneously at a higher temperature either. Figure 7b shows the reaction energy profile for the vacuum decarboxylation of **4c** via Route 7. Actually, $\Delta G_{25°C} = -14.3$ kcal/mol and $G^{\ddagger}_{25°C}$ = 65.7 kcal/mol for thermal decarboxylation. This decarboxylation is expected to occur slowly at room temperature. These results suggest that the carbonyl groups of GO will not be removed spontaneously, but the carboxyl groups are expected to be reduced slowly at temperatures of 100−150 °C.[47a,48]

3.4. Temperature Effect on GO Reduction. Reports of experimental studies have described the importance of temperature in the deoxygenation of GO. A recent study by Yang et al.[49] has demonstrated that the increase of temperature improves the efficiency of thermal reduction considerably. Thermal annealing of GOs at 500, 700, and 900 °C respectively yielded CMGs with C:O ratios of 8.9, 13.2, and 14.1.[49] Tung et al.[48] and Stankovich et al.[47a] also reported the importance of thermal annealing.

As described above, epoxide (hydroxyl) groups located at the interior of an aromatic domain of GO can be eliminated by using hydrazine (thermally annealing) with relative ease, but those located at the edges of GO are difficult to remove (see Sections 3.1 and 3.2). Therefore, epoxides and hydroxyls at the edges of aromatic domain deserve special attention. Figure 8a presents the reaction energy profile for the hydrazine de-epoxidation of **5b** via Route 2 for various temperatures. When the temperature increases from −175 to 1125 °C, ΔG decreases from −10 to −60 kcal/mol. The value of $G_1^{\ddagger}$ for the first step of reaction increases from 40 to 100 kcal/mol (Figure 8a). That increase in $G_1^{\ddagger}$ results from the fact that the first step in the reaction relies upon the capture of a hydrazine molecule on the moiety **5b** ($\Delta S < 0$). An increased temperature reduces the probability for such capturing; consequently, it will not improve the efficiency of hydrazine de-epoxidation. Figure 8b presents the reaction energy profile for the thermal dehydroxylation of **5h** via Route 5 at various temperatures. When the temperature increases, the ΔG decreases from positive to negative (Figure 8b). The critical temperature (T_c), defined as the point at ΔG = 0, is 650 °C, showing that raising the temperature will make the dehydroxylation of GO spontaneous. When the temperature is greater than 650 °C,[49] even the hydroxyls attached to the edges of GO can be readily removed.

As for the thermal decarboxylation of **4c** via Route 7, an increase in temperature will reduce ΔG without increasing the reaction energy barrier. Raising temperatures is therefore going to facilitate the thermal decarboxylation of GO as well. Although a rise in temperature is also expected to expedite thermal decarbonylation of **6b** via Route 6, the corresponding T_c is as high as 1730 °C. After thermal annealing at about 1000 °C,[49] the GO's carboxyl groups will be removed, but GO's carbonyl groups will remain. Given the opposite temperature dependences of hydrazine de-epoxidation and thermal dehydroxylation/decarboxylation, it is necessary to perform these two types of

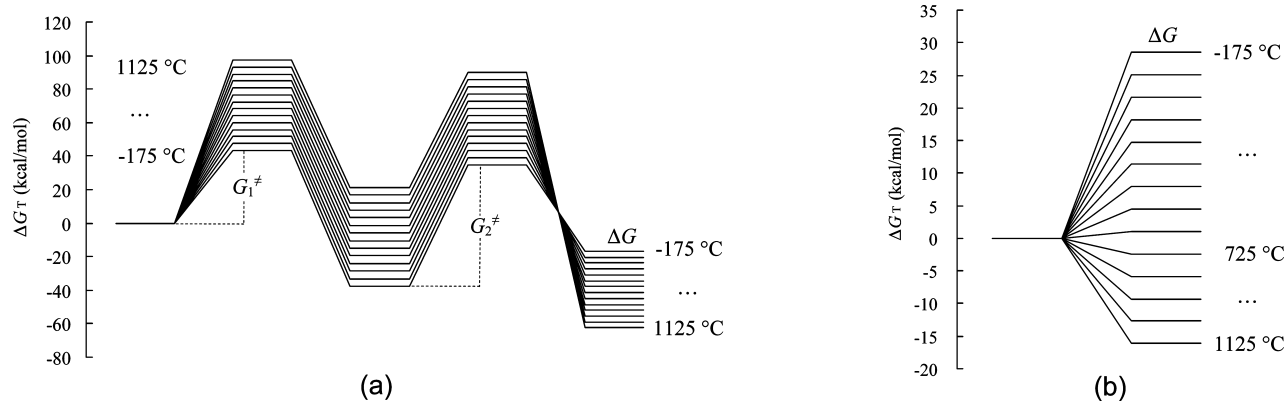

Figure 8. Relative Gibbs free energies (G_{rel}s) for stationary points involved in (a) hydrazine de-epoxidation of **5b** and (b) thermal dehydroxylation of **5h** at 14 different temperatures: −175.0, −75.0, 25.0, ..., 1125.0 °C.

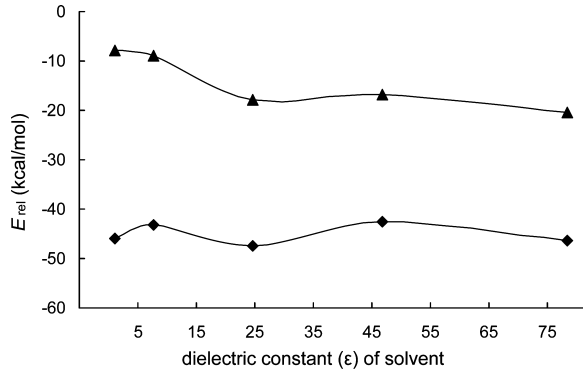

Figure 9. Relative energies for **5** + N_2H_2 + H_2O (▲) and $\mathbf{int_1}$(**5b**) (□) under vacuum and in solvents. Energies are shown in gas (ε = 1.0) and in solvents of THF (ε = 7.6), ethanol (ε = 24.6), DMSO (ε = 46.7), and water (ε = 78.4). The energies are shown as relative to the energies of isolated reactants (**5b** + N_2H_4) that were calculated with the same conditions for the solvent.

reductions for GO separately, at low and high temperatures, respectively, for high deoxygenation efficiency. Some combination of both types of reduction will give the best deoxygenation efficiency.

3.5. Solvent-Polarity Effect on the Hydrazine De-epoxidation of GO. Experimentally, the hydrazine reduction of GO is possible under vacuum,[49] in aqueous solutions,[47a] and in anhydrous hydrazine.[48] To evaluate the influence of solvent polarity, we investigated solvent effects for the de-epoxidation of **5b** via Route 2. Figure 9 presents relative energies for the deoxygenated product (**5** + N_2H_2 + H_2O) and the hydrazino alcohol intermediate (**int**) in various solvents. When the solvent changes from gas to water, the energy difference between the intermediate and deoxygenated product decreases from 38.1 to 26.0 kcal/mol. It is apparent that the energy of the intermediate is always much lower than that of the deoxygenated product (Figure 9). Consequently, the change in solvent polarity is not going to change the reaction direction found under vacuum. In solution too, the hydrazine reduction for epoxides located at the edges of an aromatic domain will be suspended by the formation of hydrazino alcohol. A base solution[29] and concentrated sulfuric acid[36b] are also known to cause deoxygenation of GO considerably. Such deoxygenations can be ascribed to the reactions between GO and solvent molecules. However, these reactions are not considered in this report.

3.6. Characterization of the Residual Groups of CMG. CMGs obtained from the reduction of GOs with hydrazine suffer from the presence of N-containing species with an atomic ratio

TABLE 3: Status of Oxygen-Containing Groups upon Treatment of Hydrazine and Heat

groups[a]	hydrazine[b]	heat[c]	hydrazine[b] and heat[c]
A	removed	not removed	removed
A′	converted to hydrazino alcohol	not removed	not removed
B	removed	removed	removed
B′	not removed	removed	removed
C	not removed	not removed	not removed
D	partly removed	removed	removed

[a] See Figure 2 for the definition of each oxygen functionality. [b] Hydrazine treatment at room temperature. [c] Thermal annealing at temperatures of 700−1200 °C.

N:C of approximately 0.058 (Table 1).[47a,48,49] The chemical compositions for the N-containing compounds remain unclear.

In view of the results presented in Sections 3.1−3.3, the N-containing compounds might be hydrazino alcohols formed by the reactions of hydrazine with (i) epoxides that are located at the edge of GO via Route 2 and (ii) epoxides that are sticking out of GO via Route 1 (Scheme 2). Epoxides of the second type are rare in GO.[41,42] Therefore, the hydrazino alcohols formed by the hydrazine reaction of the first type are expected to be responsible for the N-containing compounds observed experimentally. In contrast to this, Stankovich et al.[47a] recently proposed that the N-containing compounds might be amino-aziridines formed by the reaction of hydrazine with epoxides via Scheme 1. We did not find this mechanism (see above); instead, we located an alternative pathway, Route 2′, for the formation of amino-aziridines through the reactions of hydrazine and epoxides (Scheme 2). Scheme 2 shows that Routes 2 and 2′ are identical in the first H-transfer step but that they subsequently deviate from one another. For comparison, we calculated the energy profile for the reaction of hydrazine with **4a** via Route 2′ (Figure S2 in the SI). The values of $G^{\ddagger}_{25°C}$ and $\Delta G_{25°C}$ for Route 2′ are 33.4 and −4.1 kcal/mol, respectively (Figure S2 in the SI); $G^{\ddagger}_{25°C}$ and $\Delta G_{25°C}$ for the deoxygenation via Route 2 are respectively 17.5 and −57.0 kcal/mol (Table 2). Therefore, the formation of amino-aziridine via Route 2′ is much less competitive than the de-epoxidation via Route 2 for the reaction of **4a** with hydrazine. For the reaction of **1b** (**4b**) with hydrazine, $\Delta G_{25°C}$ for the formation of amino-aziridine is only −8.8 (−4.5) kcal/mol. $\Delta G_{25°C}$ for the formation of hydrazine alcohol is −24.1 (−20.7) kcal/mol. The formation of hydrazino alcohol is therefore much more likely than that of amino-aziridine in the reactions of **1b** and **4b** with hydrazine, which suggests that the N-containing species observed in CMGs[47a,48,49] are not amino-aziridines.

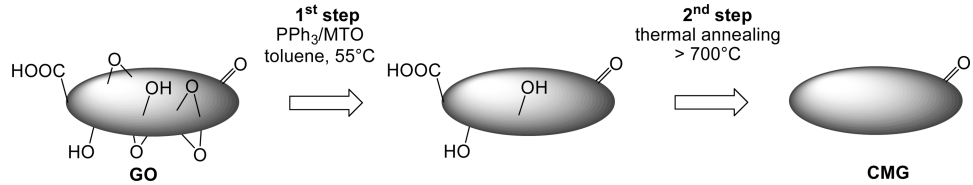

Figure 10. A two-step chemical reduction route toward the synthesis of CMG from GO.

Table 3 presents the response of oxygen functionalities of GO to hydrazine treatment, heat treatment, and their combination. To summarize, the residual groups of CMG prepared through the hydrazine reduction of GO at room temperature are **B′**, **C′**, and hydrazino alcohols converted from **A′**, and probably **D**. The residual groups of CMG prepared through the thermal annealing of GO at temperatures of 700−1200 °C are **A**, **A′**, and **C**. In fact, **A′** and **C** are only residual groups of CMGs obtained from the hydrazine reduction of GO followed by thermal annealing at temperatures of 700−1200 °C

3.7. Procedures Designed for the Reduction of GO. After hydrazine and heat treatments, epoxide groups located at the edges of aromatic domains (**A′**) and carbonyl groups (**C**) remain (Table 3). Considering the abundance of **A′** in GO,[41,42] it is desirable to investigate methods for its reduction. Recently, Billups et al. reported that epoxides on graphitic surfaces,[62,63] including those at the edges of graphite,[63] can be removed selectively with PPh_3 as a reducing agent and $MeReO_3$ (MTO) as a catalyst (at 55 °C in toluene). We studied the reaction of **2b** with MTO/PPh_3 to examine the performance of MTO/PPh_3 in the de-epoxidation of GO. Our results show that the de-epoxidation of **2b** proceeds in three steps. The Gibbs free-energy barrier for the rate-determinant step is 36.3 kcal/mol (Figure S3 of the SI), which is lower than that for the hydrazine de-epoxidation of **2b** (44.0 kcal/mol, Table 2). Consequently, the MTO/PPh_3 system is expected to perform better than hydrazine in the de-epoxidation of GO and is recommended for use.

A two-step chemical reduction route can be designed for the synthesis of CMG from GO (Figure 10): (i) treating GO with PPh3/MOT at 55 °C in toluene to remove the epoxides and (ii) thermal annealing at temperatures >700 °C to eliminate the hydroxyls and carboxyls. During preparation of this manuscript, we noted that a stepwise reduction approach had indeed been devised and implemented for GO: a reduction of GO with $NaBH_4$ at 80 °C and subsequent treatment with concentrated sulfuric acid at 180 °C followed by thermal annealing at 1100 °C.[36b] The authors reported that their stepwise reduction approach gives a deoxygenation efficiency that is higher than reduction with hydrazine or heat as the sole treatment. They reasoned that the first and the second steps contribute respectively to de-epoxidation and dehydroxylation.[36b] A combination of de-epoxidation and dehydroxylation is the necessary strategy of their stepwise reduction approach,[36b] and accords with our design for reduction procedures in Figure 10.

4. Conclusion

We located three reaction mechanisms—Routes 1, 2, and 3—for de-epoxidation of GO with hydrazine treatment (Scheme 2). Routes 2 and 3 are dominant mechanisms for epoxides attached to the aromatic domain of GO, and Route 1 is the exclusive mechanism for epoxides protruding from GO. No reaction path has been determined for reductions of hydroxyl, carbonyl, or carboxyl groups of GO with hydrazine as a reducing agent. A high-temperature thermal annealing eliminates hydroxyl and carboxyl groups from GO. The thermal dehydroxylation and decarboxylation respectively follow Routes 5 and 7.

The hydrazine reductions of epoxide groups attached to the interior of an aromatic domain of GO are thermodynamically spontaneous and have Gibbs free-energy barriers <48.3 kcal/mol at room temperature. In contrast, the hydrazine reduction of an epoxide located at the edges of an aromatic domain is blocked by the formation of a hydrazino alcohol via the first step in Route 2. These hydrazino alcohols are thermodynamically more stable than the corresponding de-epoxidation products at room temperature. Similarly, the thermal reductions of hydroxyls attached to the interior of an aromatic domain are easier than those at the edges of the aromatic domain. Regarding hydrazine de-epoxidations, raising the reaction temperature increases the Gibbs free-energy barrier. Therefore, it is not going to facilitate hydrazine de-epoxidation. An increased temperature is, however, advantageous for the thermal dehydroxylation of GO. At temperatures higher than approximately 700 °C, hydroxyl groups, including those at the edges of aromatic domains, are eliminated from GO. The residual groups of CMGs are presented in Table 3.

For improved reduction efficiency for GO, hydrazine de-epoxidation and thermal dehydroxylation should be performed separately at low and high temperatures. The combination of both types of reductions will give the best deoxygenation efficiency. The use of MTO/PPh_3 as a reducing agent is expected to improve the efficiency of de-epoxidation for GO. Figure 10 portrays the reaction procedure designed for GO reduction.

Acknowledgment. This work was supported by a Grant-in-Aid for Scientific Research on Priority Areas and for the Next Generation Super Computing Project (Nanoscience Program) from MEXT, Japan.

Supporting Information Available: The reaction route for hydrazine addition to the double bond of carbonyl (Figure S1); energy profile for the reaction of **4a** with hydrazine via Route 2′ (Figure S2); reaction energy profile for the reaction of **2b** with MTO/PPh_3 (Figure S3); intrinsic reaction coordinates (Figure S4); full citation of ref 54; calculated total energies, enthalpies, Gibbs free energies, entropies, and zero-point energies for species studied in this work (Table S1); and calculated Cartesian coordinates for species studied in this work (Table S2). This material is available free of charge via the Internet at http://pubs.acs.org.

References and Notes

(1) Wallace, P. R. *Phys. Rev.* **1947**, *71*, 622.
(2) Novoselov, K. S.; Geim, A. K.; Morozov, S. V.; Jiang, D.; Zhang, Y.; Dubonos, S. V.; Grigorieva, I. V.; Firsov, A. A. *Science* **2004**, *306*, 666.
(3) Geim, A. K.; Novoselov, K. S. *Nat. Mater.* **2007**, *6*, 183.
(4) Service, R. F. *Science* **2009**, *324*, 875.
(5) Geim, A. K. *Science* **2009**, *19*, 1530.
(6) Lee, C.; Wei, X.; Kysar, J. W.; Hone, J. *Science* **2008**, *321*, 385.
(7) Chae, H. K.; Siberio-Pérez, D. Y.; Kim, J.; Go, Y.; Eddaoudi, M.; Matzger, A. J.; O'Keeffe, M.; Yaghi, O. M. *Nature* **2004**, *427*, 523.

(8) Morozov, S. V.; Novoselov, K. S.; Katsnelson, M. I.; Schedin, F.; Elias, D. C.; Jaszczak, J. A.; Geim, A. K. *Phys. Rev. Lett.* **2008**, *100*, 016602.
(9) (a) Son, Y. W.; Cohen, M. L.; Louie, S. G. *Nature* **2006**, *444*, 347. (b) Son, Y.-S.; Cohen, M. L.; Louie, S. G. *Phys. Rev. Lett.* **2006**, *97*, 216803. (c) Han, M. Y.; Özyilmaz, B.; Zhang, Y.; Kim, P. *Phys. Rev. Lett.* **2007**, *98*, 206805. (d) Yang, L.; Park, C.-H.; Son, Y.-W.; Cohen, M. L.; Louie, S. G. *Phys. Rev. Lett.* **2007**, *99*, 186801. (e) Gorjizadeh, N.; Farajian, A. A.; Esfarjani, K.; Kawazoe, Y. *Phys. Rev. B* **2008**, *78*, 155427. (f) Topsakal, M.; Aktürk, E.; Sevinçli, H.; Ciraci, S. *Phys. Rev. B* **2008**, *78*, 235435. (g) Barone, V.; Hod, O.; Scuseria, G. E. *Nano Lett.* **2006**, *6*, 2748. (h) Rudberg, E.; Sałłek, P.; Luo, Y. *Nano Lett.* **2007**, *7*, 2211. Zhang, X. W.; Yang, G. W. *J. Phys. Chem. C* **2009**, *113*, 4662. (i) Lu, Y. H.; Chen, W.; Feng, Y. P.; He, P. M. *J. Phys. Chem. B* **2009**, *113*, 2. (j) Dalosto, S. D.; Levine, Z. H. *J. Phys. Chem. C* **2008**, *112*, 8196.
(10) Jia, X.; Hofmann, M.; Meunier, V.; Sumpter, B. G.; Campos-Delgado, J.; Romo-Herrera, J. M.; Son, H.; Hsieh, Y. P.; Reina, A.; Kong, J.; Terrones, M.; Dresselhaus, M. S. *Science* **2009**, *323*, 1701.
(11) (a) Fujita, M.; Wakabayashi, K.; Nakada, K.; Kusakabe, K. *J. Phys. Soc. Jpn.* **1996**, *65*, 1920. (b) Ezawa, M. *Phys. Rev. B* **2007**, *76*, 245415. (c) Ezawa, M. *Phys. E* **2008**, *40*, 1421. (d) Yazyev, O. V.; Wang, W. L.; Meng, S.; Kaxiras, E. *Nano Lett.* **2008**, *8*, 766. (e) Wang, W. L.; Meng, S.; Kaxiras, E. *Nano Lett.* **2008**, *8*, 241. (f) Fernández-Rossier, J.; Palacios, J. J. *Phys. Rev. Lett.* **2007**, *99*, 177204. (g) Yazyev, O. V.; Helm, L. *Phys. Rev. B* **2007**, *75*, 125408. (h) Kumazaki, H.; Hirashima, D. S. *J. Phys. Soc. Jpn.* **2007**, *76*, 064713. (i) Palacios, J. J.; Fernández-Rossier, J.; Brey, L. *Phys. Rev. B* **2008**, *77*, 195428. (j) Yazyev, O. V. *Phys. Rev. Lett.* **2008**, *101*, 037203. (k) Jiang, D.; Sumpter, B. G.; Dai, S. *J. Chem. Phys.* **2007**, *127*, 124703. (l) Gao, X.; Wang, L.; Ohtsuka, Y.; Jiang, D.; Zhao, Y.; Nagase, S.; Chen, Z. *J. Am. Chem. Soc.* **2009**, *131*, 9663.
(12) (a) Wang, Y.; Huang, Y.; Song, Y.; Zhang, X.; Ma, Y.; Liang, J.; Chen, Y. *Nano Lett.* **2009**, *9*, 220. (b) Han, K. H.; Spemann, D.; Esquinazi, P.; Höhne, R.; Riede, V.; Butz, T. *Adv. Mater.* **2003**, *15*, 1719. (c) Esquinazi, P.; Spemann, D.; Höhne, R.; Setzer, A.; Han, K. H.; Butz, T. *Phys. Rev. Lett.* **2003**, *91*, 227201.
(13) (a) Stoller, M. D.; Park, S.; Zhu, Y.; An, J.; Ruoff, R. S. *Nano Lett.* **2008**, *8*, 3498. (b) Si, Y.; Samulski, E. T. *Chem. Mater.* **2008**, *20*, 6792. (c) Yoo, E.; Kim, J.; Hosono, E.; Zhou, H.-S.; Kudo, T.; Honma, I. *Nano Lett.* **2008**, *8*, 2277.
(14) (a) Fowler, J. D.; Allen, M. J.; Tung, V. C.; Yang, Y.; Kaner, R. B.; Weiller, B. H. *ACS Nano* **2009**, *3*, 301. (b) Ang, P. K.; Chen, W.; Wee, A. T. S.; Loh, K. P. *J. Am. Chem. Soc.* **2008**, *130*, 14392. (c) Mohanty, Ni.; Berry, V. *Nano Lett.* **2008**, *8*, 4469. (d) Wehling, T. O.; Novoselov, K. S.; Morozov, S. V.; Vdovin, E. E.; Katsnelson, M. I.; Geim, A. K.; Lichtenstein, A. I. *Nano Lett.* **2008**, *8*, 173. (e) Dan, Y.; Lu, Y.; Kybert, N. J.; Luo, Z.; Johnson, A. T. C. *Nano Lett.* **2009**, *9*, 1472. (f) Rangel, N. L.; Seminario, J. M. *J. Phys. Chem. A* **2008**, *112*, 13699. (g) Huang, B.; Li, Z.; Liu, Z.; Zhou, G.; Hao, S.; Wu, J.; Gu, B.-L.; Duan, W. *J. Phys. Chem. C* **2008**, *112*, 13442.
(15) (a) Inanc, M.; Han, M. Y.; Young, A. F.; Ozyilmaz, B.; Kim, P.; Shepard, K. L. *Nat. Nanotechnol.* **2008**, *3*, 654. (b) Avouris, P.; Chen, Z.; Perebeinos, V. *Nat. Nanotechnol.* **2007**, *2*, 605. (c) Stampfer, C.; Schurtenberger, E.; Molitor, F.; Güttinger, J.; Ihn, T.; Ensslin, K. *Nano Lett.* **2008**, *8*, 2378. (d) Freitag, M.; Steiner, M.; Martin, Y.; Perebeinos, V.; Chen, Z.; Tsang, J. C.; Avouris, P. *Nano Lett.* **2009**, *9*, 1883. (e) Xia, F.; Mueller, T.; Golizadeh-Mojarad, R.; Freitag, M.; Lin, Y.-M.; Tsang, J.; Perebeinos, V.; Avouris, P. *Nano Lett.* **2009**, *9*, 1039. (f) Zhao, P.; Chauhan, J.; Guo, J. *Nano Lett.* **2009**, *9*, 684. (g) Romero, H. E.; Shen, N.; Joshi, P.; Gutierrez, H. R.; Tadigadapa, S. A.; Sofo, J. O.; Eklund, P. C. *ACS Nano* **2008**, *2*, 2037. (h) Wang, X.; Ouyang, Y.; Li, X.; Wang, H.; Guo, J.; Dai, H. *Phys. Rev. Lett.* **2008**, *100*, 206803. (i) Muñoz-Rojas, F.; Fernández-Rossier, J.; Brey, L.; Palacios, J. *J. Phys. Rev. B* **2008**, *77*, 045301. (j) Gorbachev, R. V.; Mayorov, A. S.; Savchenko, A. K.; Horsell, D. W.; Guinea, F. *Nano Lett.* **2008**, *8*, 1995. (k) Li, X.; Wang, X.; Zhang, L.; Lee, S.; Dai, H. *Science* **2008**, *319*, 1229. (l) Wang, X.; Li, X.; Zhang, L.; Yoon, Y.; Weber, P. K.; Wang, H.; Guo, J.; Dai, H. *Science* **2009**, *324*, 768.
(16) Lin, Y.; Jenkins, K. A.; Valdes-Garcia, A.; Small, J. P.; Farmer, D. B.; Avouris, P. *Nano Lett.* **2009**, *9*, 422.
(17) Pang, S.; Tsao, H. N.; Feng, X.; Müllen, K. *Adv. Mater.* **2009**, *21*, 1.
(18) (a) Burghard, M.; Klauk, H.; Kern, K. *Adv. Mater.* **2009**, *21*, 1. (b) Allen, M. J.; Tung, V. C.; Kaner, R. B. *Chem. Rev.* and references cited therein. DOI: 10.1021/cr900070d. Published Online July 17, 2009.
(19) Park, S.; Ruoff, R. S. *Nat. Nanotechnol.* **2009**, *4*, 217.
(20) Müllen, K.; Rabe, J. P. *Acc. Chem. Res.* **2008**, *41*, 511.
(21) Choucair, M.; Thordarson, P.; Stride, J. A. *Nat. Nanotechnol.* **2009**, *4*, 30.
(22) Stankovich, S.; Dikin, D. A.; Dommett, G. H. B.; Kohlhaas, K. M.; Zimney, E. J.; Stach, E. A.; Piner, R. D.; Nguyen, S. T.; Ruoff, R. S. *Nature* **2006**, *442*, 282.
(23) (a) Obraztsov, A. N. *Nat. Nanotechnol.* **2009**, *4*, 212. (b) Jin, Z.; Lomeda, J. R.; Price, B. K.; Lu, W.; Zhu, Y.; Tour, J. M. *Chem. Mater.* **2009**, *21*, 3045.
(24) Williams, G.; Seger, B.; Kamat, P. V. *ACS Nano* **2008**, *2*, 1487.
(25) Wang, X.; Zhi, L.; Müllen, K. *Nano Lett.* **2008**, *8*, 323.
(26) Su, Q.; Pang, S.; Alijani, V.; Li, C.; Feng, X.; Müllen, K. *Adv. Mater.* **2009**, *21*, 1.
(27) Allen, M. J.; Tung, V. C.; Gomez, L.; Xu, Z.; Chen, L.-M.; Nelson, K. S.; Zhou, C.; Kaner, R. B.; Yang, Y. *Adv. Mater.* **2009**, *21*, 2098.
(28) Liang, Y.; Wu, D.; Feng, X.; Müllen, K. *Adv. Mater.* **2009**, *21*, 1679.
(29) Fan, X.; Peng, W.; Li, Y.; Li, X.; Wang, S.; Zhang, G.; Zhang, F. *Adv. Mater.* **2008**, *20*, 4490.
(30) Liu, Z.; Liu, Q.; Huang, Y.; Ma, Y.; Yin, S.; Zhang, X.; Sun, W.; Chen, Y. *Adv. Mater.* **2008**, *20*, 3924.
(31) Chen, H.; Müller, M. B.; Gilmore, K. J.; Wallace, G. G.; Li, D. *Adv. Mater.* **2008**, *20*, 3557.
(32) Sundaram, R. S.; Gómez-Navarro, C.; Balasubramanian, K.; Burghard, M.; Kern, K. *Adv. Mater.* **2008**, *20*, 3050.
(33) Jung, I.; Dikin, D. A.; Piner, R. D.; Ruoff, R. S. *Nano Lett.* **2008**, *8*, 4283.
(34) Gómez-Navarro, C.; Burghard, M.; Kern, K. *Nano Lett.* **2008**, *8*, 2045.
(35) Eda, G.; Fanchini, G.; Chhowalla, M. *Nat. Nanotechnol.* **2008**, *3*, 270.
(36) (a) Gilje, S.; Han, S.; Wang, M.; Wang, K. L.; Kaner, R. B. *Nano Lett.* **2007**, *7*, 3394. (b) Gao, W.; Alemany, L. B.; Ci, L.; Ajayan, P. M. *Nat. Chem.* **2009**, *1*, 403. (c) Cote, L. J.; Cruz-Silva, R.; Huang, J. *J. Am. Chem. Soc.* **2009**, *131*, 11027. (d) Shen, J.; Hu, Y.; Shi, M.; Lu, M.; Qin, C.; Li, C.; Ye, M. *Chem. Mater.* **2009**, *21*, 3154. (e) Wang, Z.; Zhou, X.; Zhang, J.; Boey, F.; Zhang, H. *J. Phys. Chem. C* **2009**, *113*, 14071. (f) Lee, V.; Whittaker, L.; Jaye, C.; Baroudi, K. M.; Fischer, D. A.; Banerjee, S. *Chem. Mater.* **2009**, *21*, 3905.
(37) Robinson, J. T.; Perkins, F. K.; Snow, E. S.; Wei, Z.; Sheehan, P. E. *Nano Lett.* **2008**, *8*, 3137.
(38) Watcharotone, S.; Dikin, D. A.; Stankovich, S.; Piner, R.; Jung, I.; Dommett, G. H. B.; Evmenenko, G.; Wu, S. E.; Chen, S. F.; Liu, C. P.; Nguyen, S. T.; Ruoff, R. S. *Nano Lett.* **2007**, *7*, 1888.
(39) Chen, C.; Yang, Q.-H.; Yang, Y.; Lv, W.; Wen, Y.; Hou, P.-X.; Wang, M.; Cheng, H.-M. *Adv. Mater.* **2009**, *21*, 1.
(40) Jung, I.; Dikin, D.; Park, S.; Cai, W.; Mielke, S. L.; Ruoff, R. S. *J. Phys. Chem. C* **2008**, *112*, 20264.
(41) (a) Szabó, T.; Berkesi, O.; Forgo, P.; Josepovits, K.; Sanakis, Y.; Petridis, D.; Dékány, I. *Chem. Mater.* **2006**, *18*, 2740. (b) He, H.; Riedl, T.; Lerf, A.; Klinowski, J. *J. Phys. Chem.* **1996**, *100*, 19954. (c) Lerf, A.; He, H.; Riedl, T.; Forster, M.; Klinowski, J. *Solid State Ionics* **1997**, *101*−*103*, 857. (d) He, H.; Klinowski, J.; Forster, M.; Lerf, A. *Chem. Phys. Lett.* **1998**, *287*, 53. (e) Lerf, A.; He, H.; Forster, M.; Klinowski, J. *J. Phys. Chem. B* **1998**, *102*, 4477. (f) Szabó, T.; Berkesi, O.; Dékány, I. *Carbon* **2005**, *43*, 3181. (g) Szabó, T.; Tombácz, E.; Illés, E.; Dékány, I. *Carbon* **2006**, *44*, 537. (h) Aragon de la Cruz, F.; Cowley, J. M. *Nature* **1962**, *196*, 468.
(42) Cai, W.; Piner, R. D.; Stadermann, F. J.; Park, S.; Shaibat, M. A.; Ishii, Y.; Yang, D.; Velamakanni, A.; An, S. J.; Stoller, M.; An, J.; Chen, D.; Ruoff, R. S. *Science* **2008**, *321*, 1815.
(43) (a) Boukhvalov, D. W.; Katsnelson, M. I. *J. Am. Chem. Soc.* **2008**, *130*, 10697. (b) Li, Z.; Zhang, W.; Luo, Y.; Yang, J.; Hou, J. *J. Am. Chem. Soc.* **2009**, *131*, 6320.
(44) Paredes, J. I.; Villar-Rodil, S.; Solís-Fernández, P.; Martínez-Alonso, A.; Tascón, J. M. D. *Langmuir* **2009**, *25*, 5957.
(45) (a) Gómez-Navarro, C.; Weitz, R. T.; Bittner, A. M.; Scolari, M.; Mews, A.; Burghard, M.; Kern, K. *Nano Lett.* **2007**, *7*, 3499. (b) Mkhoyan, K. A.; Contryman, A. W.; Silcox, J.; Stewart, D. A.; Eda, G.; Mattevi, C.; Miller, S.; Chhowalla, M. *Nano Lett.* **2009**, *9*, 1058.
(46) Wang, G.; Yang, J.; Park, J.; Gou, X.; Wang, B.; Liu, H.; Yao, J. *J. Phys. Chem. C* **2008**, *112*, 8192.
(47) (a) Stankovich, S.; Dikin, D. A.; Piner, R. D.; Kohlhaas, K. A.; Kleinhammes, A.; Jia, Y.; Wu, Y.; Nguyen, S. T.; Ruoff, R. S. *Carbon* **2007**, *45*, 1558. (b) Kim, M. C.; Hwang, G. S.; Ruoff, R. S. *J. Chem. Phys.* **2009**, *131*, 064704.
(48) Tung, V. C.; Allen, M. J.; Yang, Y.; Kaner, R. B. *Nat. Nanotechnol.* **2009**, *4*, 25.
(49) Yang, D.; Velamakanni, A.; Bozoklu, G.; Park, S.; Stoller, M.; Piner, R. D.; Stankovich, S.; Jung, I.; Field, D. A.; Ventrice, C. A., Jr.; Ruoff, R. S. *Carbon* **2009**, *47*, 145.
(50) Mermoux, M.; Chabre, Y.; Rousseau, A. *Carbon* **1991**, *29*, 469.
(51) Li, J. L.; Kudin, K. N.; McAllister, M. J.; Prud'homme, R. K.; Aksay, I. A.; Car, R. *Phys. Rev. Lett.* **2006**, *96*, 176101.
(52) (a) Frankcombe, T. J.; Bhatia, S. K.; Smith, S. C. *Carbon* **2002**, *40*, 2341. (b) Frankcombe, T. J.; Smith, S. C. *Carbon* **2004**, *42*, 2921. (c) Sendt, K.; Haynes, B. S. *J. Phys. Chem. C* **2007**, *111*, 5465. (d) Chen, N.; Yang, R. T. *J. Phys. Chem. A* **1998**, *102*, 6348. (e) Tachikawa, H.; Kawabata, H. *J. Phys. Chem. C* **2009**, *113*, 7603. (f) Patchkovskii, S.; Tse, J. S.; Yurchenko, S. N.; Zhechkov, L.; Heine, T.; Seifert, G. *Proc. Natl. Acad. Sci. U.S.A.* **2005**, *102*, 10439.
(53) (a) Radovic, L. R.; Bockrath, B. *J. Am. Chem. Soc.* **2005**, *127*, 5917. (b) Jiang, D. E.; Sumpter, B. G.; Dai, S. *J. Chem. Phys.* **2007**, *126*,

134701. (c) Gao, X.; Zhou, Z.; Zhao, Y.; Nagase, S.; Zhang, S. B.; Chen, Z. *J. Phys. Chem. C* **2008**, *112*, 12677.
(54) Frisch, M. J. *Gaussian03*; Gaussian, Inc., Wallingford, CT, 2004.
(55) Zhao, Y.; Schultz, N. E.; Truhlar, D. G. *J. Chem. Theory Comput.* **2006**, *2*, 364.
(56) Hehre, W. J.; Ditchfield, R.; Pople, J. A. *J. Chem. Phys.* **1972**, *56*, 2257.
(57) Hariharan, P. C.; Pople, J. A. *Mol. Phys.* **1974**, *27*, 209.
(58) Cossi, M.; Rega, N.; Scalmani, G.; Barone, V. *J. Chem. Phys.* **2002**, *117*, 43.
(59) Noga, J.; Bartlett, R. J. *J. Chem. Phys.* **1987**, *86*, 7041.
(60) Dunning, T. H., Jr. *J. Chem. Phys.* **1989**, *90*, 1007.
(61) Xu, S. C.; Irle, S.; Musaev, D. G.; Lin, M. C. *J. Phys. Chem. C* **2007**, *111*, 1355.
(62) Ogrin, D.; Chattopadhyay, J.; Sadana, A. K.; Billups, W. E.; Barron, A. R. *J. Am. Chem. Soc.* **2006**, *128*, 11322.
(63) Chattopadhyay, J.; Mukherjee, A.; Hamilton, C. E.; Kang, J.; Chakraborty, S.; Guo, W.; Kelly, K. F.; Barron, A. R.; Billups, W. E. *J. Am. Chem. Soc.* **2008**, *130*, 5414.

JP909284G